Multi-objective optimal control problems using reachability analysis

Nikolaus Vertovec, Sina Ober-Blöbaum and Kostas Margellos,

***Abstract*—One of the fundamental problems in spacecraft trajectory design is finding the optimal transfer trajectory that minimizes the propellant consumption and transfer time simultaneously. We formulate this as a multi-objective optimal control (MOC) problem that involves optimizing over the initial or final state, subject to state constraints. Drawing on recent developments in reachability analysis subject to state constraints, we show that the proposed MOC problem can be stated as an optimization problem subject to a constraint that involves the sub-level set of the viscosity solution of a quasi-variational inequality. We then generalize this approach to account for more general optimal control problems in Bolza form. We relate these problems to the Pareto front of the developed multi-objective programs. The proposed approach is demonstrated on two low thrust orbital transfer problems around a rotating asteroid.**

***Index Terms*—Optimal control; Reachability analysis; Multi-objective optimization; Pareto optimality; Hamilton-Jacobi equations.**

I. Introduction

Since the Galileo mission in 1991 we have seen a steady increase in proposed missions to asteroids and comets, as they might hold the key to many scientific questions including the origins of life on earth [1]. The Dawn mission to Vesta and Ceres proved the viability of low-thrust electric propulsion for asteroid exploration [2], [3], and it is expected that many upcoming mission will rely on similar low-thrust propulsion. While there has been significant study of interplanetary transfer trajectories using low-thrust propulsion, comparatively little research has been conducted on the trajectory design in the vicinity of asteroids. We investigate a spacecraft trajectory design problem around an asteroid, where the objective is to use minimal amounts of propellant to raise an orbit while keeping flight times as short as possible. This is a multi-objective optimal control (MOC) problem, whereby one seeks to find the optimal way a dynamical system can perform a certain task, while minimizing or maximizing a set of, usually contradictory and incommensurable, objective functions [4]. For spacecraft trajectory design, there are two possible formulations for minimizing the burnt propellant. The first assumes that the initial mass is a free optimization variable. This approach is common during mission design where the total required fuel budget is being calculated. The second approach assumes a fixed initial mass and the objective is to maximize the remaining mass after completing a given orbital maneuver. This approach is more common when the maneuver needs to be added to a given mission and the available fuel is non-negotiable.

Reaching/achieving a target while satisfying state constraints is the backbone of spacecraft trajectory design problems. To this end tools from reachability analysis are often employed. Reachability analysis aims to find the set of points from which a target can be reached within a given time, subject to constraints. It forms a fundamental part of the dynamics and control literature and has been used extensively for controller synthesis of complex systems [5]–[7]. In recent years we have seen considerable research being conducted into computing reachable sets using Hamilton-Jacobi (HJ) reachability analysis, whereby the reachable set is derived from the viscosity solution of a HJB equation accounting also for the presence of state constraints [8]–[13]. One of the advantages of using HJ reachability is that the optimal trajectory can easily be constructed once the reachable set has been computed. This makes HJ reachability attractive for problems that require computing trajectories for various different initial states. In this paper we aim at extending reachability analysis to address multi-objective optimization problems. To this end we formulate the spacecraft trajectory design problem as a MOC problem and show that it can be equivalently stated as an optimization problem subject to a constraint that involves the sub-level set of a certain value function. The latter is shown to be the unique continuous viscosity solution of a quasi-variational inequality that involves a Hamilton-Jacobi-Bellman (HJB) equation. Such value functions have been defined in [8], [10] to account for the presence of state constraints. This characterization allows characterizing the Pareto front of the formulated MOC problem, and also facilitates its computation by means of available numerical tools.

In [14] the authors propose an extension of the HJ approach to solve multi-objective optimization problems while in [15] the authors extend the approach to tackle finite-horizon control problems in spacecraft trajectory design. This paper extends that research, by looking at an alternative formulation that requires fewer states to tackle a similar problem. Using approximations of the gravity field and normalizing the state space, we are able to solve a similar problem as in [15], however, in a computationally more efficient manner. Furthermore, we generalize our proposed methods to arbitrary multi-objective optimization problems.

Since the value function needed for optimization is only computed once for all possible initial states, the presented approach can make the comparison of multiple trajectories vastly more efficient compared with typical shooting methods [16]. The proposed method is generalizable to arbitrary MOC

Nikolaus Vertovec and Kostas Margellos are with the University of Oxford. Email:{nikolaus.vertovec, kostas.margellos}@eng.ox.ac.uk.

Sina Ober-Blöbaum is with the University of Paderborn. Email:{sinaober@math.uni-paderborn.de}.

problems through the addition of an auxiliary state. Using HJ reachability to constrain optimization problems enables a new broad spectrum of possible applications, expanding the traditional framework of using HJ reachability solely for safety-critical applications.

This paper is organized into six sections. Section II contains details regarding the derivations of the spacecraft dynamics as well as the definitions of the constraints pertaining its behavior. In Section III the optimal control problem is formulated while Section IV describing how the set of admissible initial states is derived from the viscosity solution of a quasi-variational inequality. Section V is dedicated to the numerical computation and case study of an orbital transfer around a rotating asteroid. Finally, Section VI provides concluding remarks and directions for future work.

II. Mathematical description and physical modeling

A. Spacecraft equations of motion

We begin by modeling the dynamics of the spacecraft. The spacecraft thrust can be modeled using the input

$$\mathbf{u}(t) := \left[\mathbf{u}_x(t), \mathbf{u}_y(t), \mathbf{u}_z(t)\right]^T \in \mathcal{U}, \tag{1}$$

where $\mathcal{U}$ is the set of possible control input values. By $\mathbf{u} \in \mathcal{U}_{ad}$ we denote the control policy and $\mathcal{U}_{ad}$ denotes the set of admissible policies which is the set of Lebesgue measurable functions from $[0, +\infty]$ to $\mathcal{U}$. Boldface notation is used to denote trajectories and policies, while non boldface notation is used to denote scalars and vectors.

The equations of motion of the spacecraft around a rotating body can be expressed in 3-dimensional Euclidean space as a second-order ordinary differential equation (see eg., [17])

$$\begin{aligned} 2\boldsymbol{\Omega}(t) \times \frac{\partial \mathbf{R}(t)}{\partial t} + \boldsymbol{\Omega}(t) \times (\boldsymbol{\Omega}(t) \times \mathbf{R}(t)) + \frac{\partial U(\mathbf{R}(t))}{\partial \mathbf{R}} \\ + \frac{\partial \boldsymbol{\Omega}(t)}{\partial t} \times \mathbf{R}(t) - \frac{\mathbf{u}(t)}{m(t)} = -\frac{\partial^2 \mathbf{R}(t)}{\partial t^2}, \end{aligned} \tag{2}$$

where $\mathbf{R}$(t) is the radius vector from the asteroids center of mass to the particle, the first and second time derivatives of $\mathbf{R}$(t) are with respect to the body-fixed coordinate system, $U(\mathbf{R}(t))$ is the gravitational potential of the asteroid and Ω is the rotational angular velocity vector of the asteroid relative to inertial space. The term $2\boldsymbol{\Omega}(t) \times \frac{\partial \mathbf{R}(t)}{\partial t}$ describes the Coriolis forces, $\boldsymbol{\Omega}(t) \times (\boldsymbol{\Omega}(t) \times \mathbf{R}(t))$, the centrifugal forces and $\frac{\partial \boldsymbol{\Omega}(t)}{\partial t} \times \mathbf{R}(t)$ the Euler forces. We consider an asteroid rotating uniformly with constant magnitude ω around the z-axis. Therefore, the Euler forces can be neglected and we can express the rotation vector as $\Omega := \omega \cdot e_z$, where e_z is the unit vector along the z-axis. Following [18], the radius vector and its derivatives are given by

$$\mathbf{R}(t) := \begin{bmatrix} \mathbf{x}(t) \\ \mathbf{y}(t) \\ \mathbf{z}(t) \end{bmatrix}, \quad \frac{\partial \mathbf{R}(t)}{\partial t} = \begin{bmatrix} \mathbf{v}_x(t) \\ \mathbf{v}_y(t) \\ \mathbf{v}_z(t) \end{bmatrix}. \tag{3}$$

The Coriolis and centrifugal forces (the first two terms in (2)) acting on the spacecraft are thus

$$2\Omega \times \frac{\partial \mathbf{R}(t)}{\partial t} = \begin{bmatrix} -2\, \mathbf{v}_y(t) \\ 2\omega \mathbf{v}_x(t) \\ 0 \end{bmatrix}, \quad \Omega \times (\Omega \times \mathbf{R}(t)) = \begin{bmatrix} -\omega^2 \mathbf{x}(t) \\ -\omega^2 \mathbf{y}(t) \\ 0 \end{bmatrix}. \tag{4}$$

To model the current position, velocity and available propellant, we define the state vector

$$r := \left[x, y, z, v_x, v_y, v_z, \Delta m\right]^T \in \mathbb{R}^7, \tag{5}$$

where Δm denotes the available propellant. We consider a spacecraft with a dry mass m_0. Then following our derivations from (2) we can formulate the dynamics of the spacecraft as

$$\dot{r} = f(r, u) = \begin{bmatrix} v_x \\ v_y \\ v_z \\ U_x(x,y,z) + \omega^2 x + 2\omega v_y + \frac{u_x}{m_0 + \Delta m} \\ U_y(x,y,z) + \omega^2 y - 2\omega v_x + \frac{u_y}{m_0 + \Delta m} \\ U_z(x,y,z) + \frac{u_z}{m_0 + \Delta m} \\ -\frac{\sqrt{u_x^2 + u_y^2 + u_z^2}}{v_{\text{exhaust}}} \end{bmatrix}, \tag{6}$$

where v_{exhaust} is the exhaust velocity used to express the depletion of mass as propellant is burned, U_x, U_y and U_z are the derivatives of the gravitational potential in the direction of the unit vectors e_x, e_y and e_z, respectively, and where for brevity we neglect the time dependence by denoting $r = \mathbf{r}(t)$, $v_x = \mathbf{v}_x(t)$, and similarly for the other states.

B. State constraints

Since the dynamics of the spacecraft were derived for orbits in the vicinity of the asteroid, we need to enforce state constraints on x, y, z. We naturally also need to ensure that we bound the amount of propellant available. Assuming that the burnout mass of the spacecraft is the same as the dry mass, we set $m_{\min} := 0$ and $m_{\max} := m_{\text{propellant}}$ and impose $m_{\min} \leq \Delta m \leq m_{\max}$.

Due to particles ejected from the asteroid, we do not want to fall below a circular orbit with radius $\rho := \sqrt{x^2 + y^2 + z^2}$ of approximately $\rho_{\min} = 1$ km. Furthermore, we need to stay within the sphere of influence (SOI) of the asteroid. The SOI can be approximated by $\rho_{SOI} \approx a \left(\frac{M_1}{M_2}\right)^{\frac{2}{5}}$, where a is the semi-major axis of the asteroid's orbit around the sun ($1.5907 \cdot 10^8$ km), M_1 is the Mass of the asteroid ($1.4091 \cdot 10^{12}$ kg) and M_2 is the mass of the sun ($1.9890 \cdot 10^{30}$ kg). Therefore, the sphere of influence of the asteroid is approximately $\rho_{\max} = \rho_{SOI} \approx 8.74$ km. The set of states that satisfy the aforementioned restrictions is given by

$$\mathcal{K} := \left\{ r \in \mathbb{R}^7 : \rho \in [\rho_{\min}, \rho_{\max}], m \in [m_{\min}, m_{\max}] \right\}.$$

The target orbit that we would like to transfer to is denoted by the closed target set $\mathcal{C} \subset \mathcal{K}$. The initial orbit that we start at is denoted by the closed initial set $\mathcal{I} \subset \mathcal{K}$. Note that the initial and the target orbit are such that restrict the position and the velocity, but allow the mass to take any admissible value within $[m_{\min}, m_{\max}]$.

While Cartesian coordinates are useful for modeling the behavior of an object around a rotating body, since we restrict all admissible states to lie within the set $\mathcal{K}$, which constraint the radius ρ, it is more efficient to recast our problem in spherical coordinates. To this end, define a_ρ, a_θ, a_ψ as the transformations of

$$\begin{aligned} a_x &:= U_x(x,y,z) + \omega^2 x + 2\omega v_y, \\ a_y &:= U_y(x,y,z) + \omega^2 y - 2\omega v_x, \\ a_z &:= U_z(x,y,z). \end{aligned}$$

The tangential velocity in the x-y plane, v_t, and its perpendicular counterpart, $v_\perp$, can then be defined as follows:

$$\begin{bmatrix} v_t \\ v_\perp \end{bmatrix} = \begin{bmatrix} \rho\dot{\theta}\sin\psi \\ \rho\dot{\psi} \end{bmatrix}, \tag{7}$$

$$\begin{bmatrix} a_t \\ a_\perp \end{bmatrix} = \begin{bmatrix} \sin\psi[a_\theta\rho + \dot{\theta}v_\rho] + \dot{\theta}v_\perp\cos\psi \\ \rho\dot{\psi} + a_\psi\rho \end{bmatrix}. \tag{8}$$

Then we can restate the system dynamics in spherical coordinates as

$$r = \left[\rho, \theta, \psi, v_\rho, v_t, v_\psi, \Delta m\right]^T \in \mathbb{R}^7, \tag{9}$$

$$\dot{r} = \begin{bmatrix} v_\rho \\ \frac{v_t}{\rho\sin\psi} \\ \frac{v_\perp}{\rho} \\ a_\rho + \frac{T}{m_0+\Delta m}\cos\alpha \\ a_t + \frac{T}{m_0+\Delta m}\sin\alpha\sin\delta \\ a_\perp + \frac{T}{m_0+\Delta m}\sin\alpha\cos\delta \\ -\frac{T}{v_{\text{exhaust}}} \end{bmatrix}. \tag{10}$$

The input $\mathbf{u}(t)$ is redefined for spherical coordinates as $\mathbf{u}(t) := [\boldsymbol{\alpha}(t), \boldsymbol{\delta}(t), \mathbf{T}(t)] \in \mathcal{U}$, where $\boldsymbol{\alpha}(t) \in [-\pi, \pi]$ is the incidence angle, $\boldsymbol{\delta}(t) \in [-\frac{\pi}{2}, \frac{\pi}{2}]$ is the sideslip angle and $\mathbf{T}(t) \in [0, T_{\max}]$ is the variable thrust. With a slight abuse of notation we also define by $\mathcal{I}$, $\mathcal{C}$ and $\mathcal{K}$ the initial, target and constrained set of admissible states, respectively, in spherical coordinates.

III. Problem Statement

A. Multi-objective optimal control problem

Having defined the system dynamics, we are now in a position to discuss how to find trajectories that start on an initial orbit, $\mathcal{I}$, and take the spacecraft to some final orbit, $\mathcal{C}$. Additionally, the objective is to keep the flight time and required propellant as small as possible. Thus, the multi-objective optimal control problem can be formulated as a minimization problem whereby the first goal is to minimize the required propellant, Δm and the second is to minimize the required time for the orbit change, i.e. the transfer time, denoted by t_f.

The trajectory, $\mathbf{r}$, which is the solution of (10), belongs to the Sobolev space $\mathbb{W}^{1,1}(\mathbb{R}^7)$. The set of trajectory-control pairs on $[-t_f, 0]$ starting at r_0 with transfer time t_f is denoted as:

$$\begin{aligned} \Pi_{r_0,t_f} := \{(\mathbf{r},\mathbf{u}) : \dot{\mathbf{r}}(t) = f(\mathbf{r}(t),\mathbf{u}(t)), \quad t \in [-t_f, 0]; \\ \mathbf{r}(-t_f) = r_0\} \subset \mathbb{W}^{1,1}(\mathbb{R}^7) \times \mathcal{U}_{ad}. \end{aligned}$$

Note that as in [19] we adopt the convention that 0 denotes the terminal time hence the transfer time t_f denotes the time duration. The set of admissible (in the sense of satisfying the state constraints) trajectory-control pairs on $[-t_f, 0]$ starting at r_0 with transfer time t_f is denoted as:

$$\begin{aligned} \Pi^{\mathcal{K},\mathcal{C}}_{r_0,t_f} := \{(\mathbf{r},\mathbf{u}) \in \Pi_{r_0,t_f} : \mathbf{r}(t) \in \mathcal{K}, \quad t \in [-t_f, 0]; \\ \mathbf{r}(0) \in \mathcal{C}\} \subset \mathbb{W}^{1,1}(\mathbb{R}^7) \times \mathcal{U}_{ad}. \end{aligned}$$

Finally, the set of admissible initial state and transfer time pairs is denoted as

$$\pi := \{(r_0, t_f) \in \mathbb{R}^7 \times [0, +\infty) \quad \text{such that} \quad \Pi^{\mathcal{K},\mathcal{C}}_{r_0,t_f} \neq \emptyset\}.$$

For a given initial state $r_0 \in \mathbb{R}^7$ and transfer time $t_f \in [0, +\infty)$, we can define the cost functions as $J_1(r_0, t_f) := \Delta m$ and $J_2(r_0, t_f) := t_f$, where Δm is the 7-th element of the state vector r_0. The 2-dimensional objective function $J : \mathbb{R}^7 \times [0, +\infty) \to \mathbb{R}^2$ can then be written as

$$J(r_0, t_f) := \left[J_1(r_0, t_f), J_2(r_0, t_f)\right]^T. \tag{11}$$

We are now in a position to formulate the multi-objective optimal control problem under study as

$$\begin{aligned} \underset{(r_0,t_f)\in I\times[0,\infty)}{\text{minimize}} \quad & J(r_0, t_f) \\ \text{subject to} \quad & (r_0, t_f) \in \pi \end{aligned} \tag{12}$$

B. Pareto optimality

The solution of (12) in general does not consist of a single isolated point, but rather a set of optimal compromises between the objectives J_1 and J_2 [20].

More formally, a vector a is considered less than b (denoted $a < b$) if for every element a_i and b_i the relation $a_i < b_i$ holds. The relations $\leq, \geq, >$ are defined in an analogous way.

Definition 3.1: A solution (r_0, t_f) is considered Pareto optimal if $\nexists(\hat{r_0}, \hat{t}_f) \in \pi$ such that $J(\hat{r_0}, \hat{t}_f) < J(r_0, t_f)$.

Following Definition 3.1, a solution (r_0, t_f) is considered Pareto optimal if it is not possible to improve all its performance metrics $J_1(r_0, t_f), J_2(r_0, t_f)$ simultaneously. The set of Pareto optimal solutions is called the Pareto set $\mathcal{P}_S$, while its image is the Pareto front $\mathcal{P}_F$. Therefore, the solution of (12) is the desired Pareto front.

To allow for mission designers to determine a compromise between minimizing required propellant and transfer times, we wish to compute the Pareto front. However, the unconventional constraint in (12) ensuring a solution (r_0, t_f) is feasible, prevents us from solving (12) with standard MOC solvers. Therefore, we will next discuss how we can recast the constraint $(r_0, t_f) \in \pi$ to a standard nonlinear inequality constraint, which will allow us to compute the Pareto front by means of conventional MOC solvers.

IV. Solution to multi-objective optimal control problems

To find an equivalent formulation for the constraint $(r_0, t_f) \in \pi$, let $g(r)$ and $\nu(r)$ be two Lipschitz functions (with Lipschitz constants L_g and L_ν, respectively) chosen such that

$$\begin{aligned} g(r) \leq& 0 \iff r \in \mathcal{K}, \\ \nu(r) \leq& 0 \iff r \in \mathcal{C}. \end{aligned}$$

This can be achieved by choosing $g(r)$ and $\nu(r)$ as the signed distance to the set $\mathcal{K}$ and $\mathcal{C}$, respectively.

We impose the following assumptions on the spacecraft dynamics.

Assumption 4.1: For every $r \in \mathcal{K}$ the set $\Big\{f(r,u) : u \in \mathcal{U}\Big\}$ is a compact convex subset of $\mathbb{R}^7$.

Assumption 4.2: $f : \mathbb{R}^7 \times \mathcal{U} \to \mathbb{R}^7$ is bounded and there exists an $L_f > 0$ such that for every $u_1, u_2 \in \mathcal{U}$,

$$|f(r_1,u_1) - f(r_2,u_2)| \leq L_f |r_1 - r_2|.$$

Using Assumption 4.1 and 4.2, for any control policy $\mathbf{u} \in \mathcal{U}_{ad}$, any initial state $r_0 \in \mathcal{K}$ and transfer time $t_f > 0$, the system admits a unique, absolutely continuous solution on $[-t_f, 0]$ [21]. Moreover, under Assumption 4.1 and by Filippov's Theorem [22], we can conclude, that Π_{r_0,t_f} is compact.

Consider the value function ω:

$$\omega(r_0,t_f) := \inf_{(\mathbf{r},\mathbf{u})\in\Pi_{r_0,t_f}} \Big\{ \nu(\mathbf{r}(0)) \bigvee \max_{\tau\in[-t_f,0]} g(\mathbf{r}(\tau))\Big\}, \quad (13)$$

where $a \bigvee b$ denotes $\max(a,b)$.

We are now in a position to use the value function to decide if, for a given initial state and transfer time, there exists a corresponding admissible trajectory. Thus we can introduce an equivalent formulation of (12).

Theorem 4.1: The constrained MOC problem, (12), is equivalent to

$$\begin{aligned} \underset{(r_0,t_f)\in I\times[0,\infty)}{\text{minimize}} \quad & J(r_0,t_f) \\ \text{subject to} \quad & \omega(r_0,t_f) \leq 0. \end{aligned} \quad (14)$$

Proof: We show that $(r_0,t_f) \in \pi \iff \omega(r_0,t_f) \leq 0$.

Case A: Consider $(r_0,t_f) \in \pi$. For the sake of contradiction assume that $\omega(r_0,t_f) > 0$. This then implies that for all $(\mathbf{r},\mathbf{u}) \in \Pi^{\mathcal{K},\mathcal{C}}_{r_0,t_f}$ either $\nu(\mathbf{r}(0)) > 0 \iff \mathbf{r}(0) \notin \mathcal{C}$ or there exists $\tau \in [-t_f, 0]$ such that $g(\mathbf{r}(t)) > 0 \iff \mathbf{r}(t) \notin \mathcal{K}$. This contradicts the fact that $(r_0,t_f) \in \pi$ establishing that $(r_0,t_f) \in \pi$ implies $\omega(r_0,t_f) \leq 0$

Case B: Consider $(r_0,t_f) \in \mathcal{I} \times [0,\infty)$, such that $\omega(r_0,t_f) \leq 0$. Under Assumption 4.1, applying Weierstrass' Theorem on the existence of minima for compact sets [23], [24], we can conclude that the infimum over Π_{r_0,t_f} exists, and thus, $\omega(r_0,t_f) \leq 0$ implies the existence of a trajectory-control pair $(\mathbf{r},\mathbf{u}) \in \Pi_{r_0,t_f}$, such that for all $t \in [-t_f, 0]$, $g(\mathbf{r}(t)) \leq 0$ and $\nu(\mathbf{r}(0)) \leq 0$. By definition of the function g and ν, we thus have $\mathbf{r}(t) \in \mathcal{K}$ for all $t \in [-t_f, 0]$ and $\mathbf{r}(0) \in \mathcal{C}$, which in turns implies $(\mathbf{r},\mathbf{u}) \in \Pi^{\mathcal{K},\mathcal{C}}_{r_0,t_f}$. Therefore,

$$\omega(r_0,t_f) \leq 0 \Rightarrow (r_0,t_f) \in \pi,$$

thus concluding the proof. ■

Theorem 4.1 implies that the Pareto front can be computed as the solution of (14). To achieve this we discuss how to compute ω.

A. Value function computation

To begin to discuss how ω can be obtained, we introduce the Hamiltonian $H : \mathbb{R}^7 \times \mathbb{R}^7 \to \mathbb{R}$,

$$H(r,q) := -\min_{u\in\mathcal{U}} \left(f(r,u) \cdot q\right), \quad (15)$$

where $q \in \mathbb{R}^7$ is the costate vector.

Theorem 4.2: The value function ω is the unique continuous viscosity solution of the following quasi-variational inequality

$$\begin{cases} 0 = \max\left\{g(r) - \omega(r,t), \partial_t\omega + H(r,\nabla_r\omega)\right\} \\ \qquad\qquad \text{for all} \quad t \in [0,\infty),\ r \in \mathbb{R}^7, \\ \omega(r,0) = \Big(\nu(r) \bigvee g(r)\Big) \quad \text{for all} \quad r \in \mathbb{R}^7, \end{cases}$$

Since the Dynamic Programming Principle [23] holds for $h \in [0,h]$, $(r_0,t_f) \in \mathcal{K} \times \mathbb{R}$ with $h \geq 0$:

$$\omega(r_0,t_f) = \inf_{(\mathbf{r},\mathbf{u})\in\Pi_{r_0,t_f}} \Big\{\omega(\mathbf{r}(h-t_f), t_f - h) \bigvee \max_{s\in[-t_f,h-t_f]} g(\mathbf{r}(s))\Big\},$$

the proof of Theorem 4.2 follows standard arguments for viscosity solutions, as shown in [8], [24]. Note that the infimum should be understood to be over the restriction of Π_{r_0,t_f} over $[-t_f, h-t_f]$.

In order to solve the quasi-variational inequality in Theorem 4.2, we employ a finite differences scheme. To ensure convergence of the numerical solution, we make the following observation.

Proposition 4.1: The value function ω is Lipschitz continuous.

The proof is similar to the more general proof of Proposition 4.2 that is introduced in the sequel.

Using Proposition 4.1, by the Picard-Lindelöf theorem, the numerical solution of ω will converge to the true solution [25], [21].

The Hamiltonian admits an explicit form. To this end consider the term

$$C(r,q) := q_1 v_\rho + q_2 v_t + q_3 v_\perp + q_4 a_\rho + q_5 a_t + q_6 a_\perp.$$

Then we can write the Hamiltonian as follows

$$H(r,q) := -\min_{u\in\mathcal{U}} \Big(\frac{T}{m_0 + \Delta m}(q_4 \cdot \cos\alpha + \sin\alpha\left(q_5 \sin\delta + q_6\cos\delta\right)) - q_7 \cdot \frac{T}{v_{\text{exhaust}}}\Big) - C(r,q).$$

As T is always positive, we can minimize the term $(q_4 \cdot \cos\alpha + \sin\alpha\left(q_5 \cdot \sin\delta + q_6 \cdot \cos\delta\right))$ separately. We can rewrite the trigonometric functions $a\cos x + b\sin x$ as $R\cos\left(x - \arctan\frac{b}{a}\right)$ with $R = \sqrt{a^2+b^2}$. We, therefore, introduce the auxiliary variables

$$\chi(\delta) := \sqrt{q_5^2 + q_6^2} \cdot \cos\left(\delta - \arctan\frac{q_5}{q_6}\right),$$

$$A(\delta) := \sqrt{q_4^2 + \chi(\delta)^2}.$$

We can first optimize over α, and subsequently over δ (notice that this sequential minimization is exact since $A(\delta) \geq 0$). We thus have

$$\min_{\alpha,\delta\in[-\pi,\pi]\times[-\frac{\pi}{2},\frac{\pi}{2}]} \left(q_4\cos\alpha + \sin\alpha\left(q_5\sin\delta + q_6\cos\delta\right)\right)$$
$$= \min_{\delta\in[-\frac{\pi}{2},\frac{\pi}{2}]} A(\delta) \min_{\alpha\in[-\pi,\pi]} \cos\left(\alpha - \arctan\frac{\chi(\delta)}{q_4}\right).$$

This results in the optimal thrust angles

$$\alpha^*(\delta) := \pm\pi + \arctan\frac{\chi(\delta)}{q_4}.$$

Since $\cos\left(\alpha^*(\delta) - \arctan\frac{\chi(\delta)}{q_4}\right) = -1$, after applying $\alpha^*(\delta)$, it follows that

$$\delta^* \in \operatorname*{arg\,min}_{\delta\in[-\frac{\pi}{2},\frac{\pi}{2}]} -A(\delta) = \arctan\frac{q_5}{q_6} \pm \pi.$$

Subsequently,

$$q_4\cos\alpha^* + \sin\alpha^*\left(q_5\sin\delta^* + q_6\cos\delta^*\right) = -\sqrt{q_4^2+q_5^2+q_6^2}. \tag{16}$$

The results of (16) allow us to minimize with respect T, i.e.

$$H(r,q) = -\min_{T\in[0,T_{\max}]}\Big(-\frac{T}{m_0+\Delta m}\cdot\sqrt{q_4^2+q_5^2+q_6^2} - q_7\cdot\frac{T}{v_{\text{exhaust}}}\Big) - C(r,q)$$
$$\Rightarrow T^* := \begin{cases} T_{\max} & \text{if } \frac{q_7}{v_{\text{exhaust}}} + \frac{\sqrt{q_4^2+q_5^2+q_6^2}}{m_0+\Delta m} \geq 0 \\ 0 & \text{otherwise} \end{cases}.$$

Finally, applying T^* and rewriting the minimum as the maximum of the negation of the associated function, the Hamiltonian takes the following analytic form

$$H(r,q) := -C(r,q) + \max\Big(q_7\cdot\frac{T_{\max}}{v_{\text{exhaust}}} + \frac{T_{\max}}{m_0+\Delta m}\sqrt{q_4^2+q_5^2+q_6^2}, 0\Big).$$

B. Extension to problems in Bolza form

We will now generalize our approach to problems where the objective functions do not rely only on the initial state, and are written in Bolza form. To achieve this we need to introduce auxiliary states. For completeness, we show how problems in Bolza form are reformulated into Mayer form, and then show how problems in Mayer form are solved in a similar fashion as before.

Consider the p-dimensional objective function defined as:

$$J_{\text{Bolza}}(\mathbf{r},\mathbf{u},t_f) := J_{\text{t}}(\mathbf{r}(0)) + \int_{-t_f}^{0} J_{\text{r}}(\mathbf{r}(s),\mathbf{u}(s))ds. \tag{17}$$

We impose the following assumptions, as in [14].

Assumption 4.3: J_{t} is locally Lipschitz continuous on $\mathbb{R}^7$ with Lipschitz constant $L_{\text{t}}(R)$ for every neighborhood $R \subset \mathbb{R}^7$.

Assumption 4.4: J_{r} is continuous on $\mathbb{R}^7 \times \mathcal{U}$. Moreover, J_{r} is locally Lipschitz continuous on the first variable with Lipschitz constant $L_{\text{r}}(R)$ for every neighborhood $R \subset \mathbb{R}^7$.

Remark 1: To ease notation, we omit the dependents on the neighborhood for the Lipschitz constants and instead assume the existence of a global Lipschitz constant L_{t} and L_{r} respectively.

Next, we define an auxiliary state $z \in \mathbb{R}^p$ as:

$$\begin{cases} \dot{\mathbf{z}}(s) = -J_{\text{r}}(\mathbf{r}(s),\mathbf{u}(s)), & \forall s\in[-t_f,0] \\ \mathbf{z}(0) = z_0, \end{cases} \tag{18}$$

where z_0 becomes an optimization parameter and $\mathbf{z} \in \mathbb{W}^{1,1}(\mathbb{R}^p)$. The auxiliary state captures the cumulative running cost, and thus is treated as an additional state. In the same manner that we previously ensured that a trajectory, $\mathbf{r}$, stayed within the set $\mathcal{K}$, we will bound $\mathbf{z}$ and ensure that the integrated running cost, added with the terminal cost, stays below some value z_0. To capture all possible trajectories, we introduce the set

$$\mathcal{Z}_{r_0,t_f,z_0} := \{(\mathbf{r},\mathbf{u},\mathbf{z}) : (\mathbf{r},\mathbf{u})\in\Pi_{r_0,t_f}; \dot{\mathbf{z}}(s) = -J_{\text{r}}(\mathbf{r}(s),\mathbf{u}(s)), \forall s\in[-t_f,0]; \mathbf{z}(0) = z_0\}, \tag{19}$$

and make the following assumption.

Assumption 4.5: For every $r\in\mathbb{R}^7$,the set

$$\left\{\begin{bmatrix} f(r,u) \\ J_{\text{r}} \end{bmatrix} : u\in\mathcal{U},\right\}$$

is a compact convex subset of $\mathbb{R}^7\times\mathbb{R}^p$.
We now introduce the auxiliary value function ϑ:

$$\vartheta(r_0,t_f,z_0) := \inf_{(\mathbf{r},\mathbf{u},\mathbf{z})\in\mathcal{Z}_{r_0,t_f,z_0}}\Big\{ \bigvee_i J_{\text{t}}^i(\mathbf{r}(0)) - \mathbf{z}^i(-t_f) \bigvee \nu(\mathbf{r}(0)) \bigvee \max_{s\in[-t_f,0]} g(\mathbf{r}(s))\Big\}, \tag{20}$$

where $\bigvee_i x^i$ denotes the maximum element of the vector x. As with ω, the term $\max_{s\in[-t_f,0]} g(\mathbf{r}(s))$ and $\nu(\mathbf{r}(0))$ ensures that any trajectory $\mathbf{r}$ remains in $\mathcal{K}$ and terminates in $\mathcal{C}$. The additional term $J_{\text{t}}^i(\mathbf{r}(0)) - \mathbf{z}^i(-t_f)$ ensures that the integrated running cost J_{r} combined with the terminal cost J_{t} never grows larger than z_0. Thus, in addition to ensuring that $(\mathbf{r},\mathbf{u})$ are admissible trajectory control pairs, the subzero level set of ϑ bounds the terminal and integrated running cost. Therefore,

$$\vartheta(r_0,t_f,z_0)\leq 0 \iff \Big[\exists(\mathbf{r},\mathbf{u})\in\Pi_{r_0,t_f}^{\mathcal{K},\mathcal{C}}, J_{\text{Bolza}}(\mathbf{r},\mathbf{u},t_f)\leq z_0\Big]. \tag{21}$$

We are now in a position to introduce the generalized multi-objective optimal control problem for objective functions in Bolza form:

$$\begin{aligned} &\underset{(r_0,t_f)\in I\times[0,\infty)}{\text{minimize}} && z_0 \\ &\text{subject to} && \vartheta(r_0,t_f,z_0)\leq 0, \end{aligned} \tag{22}$$

where z_0 represents an upper bound for the term $J_{\text{Bolza}}(\mathbf{r},\mathbf{u},t_f)$, without explicit knowledge of $\mathbf{r}$ or $\mathbf{u}$.

The generalized value function can again be obtained as the unique continuous viscosity solution of a HJB equation

$$\begin{cases} 0 = \max\{g(r) - \vartheta(r,t,z), \partial_t \vartheta + H(r, \nabla_r \vartheta, \nabla_z \vartheta)\} \\ \qquad\qquad\qquad \text{for all} \quad t \in [0,\infty),\ r \in \mathcal{K}, z \in \mathbb{R}^p, \\ \vartheta(r,0,z) = \bigvee_i J_{\mathrm{t}}^i(r) - z^i \bigvee \nu(r) \bigvee g(r) \\ \qquad\qquad\qquad\qquad\qquad \text{for all} \quad r \in \mathcal{K}, \end{cases} \tag{23}$$

where the Hamiltonian is defined as

$$H(r, q_r, q_z) \coloneqq \min_{u \in \mathcal{U}} \left(q_r^T \cdot f(r,u) - q_z^T J_{\mathrm{r}}(r,u) \right).$$

Proposition 4.2: The value function ϑ is Lipschitz continuous.

The proof can be found in the Appendix. Proposition 4.2 can be used to show that a numerical solution of (23) (in the viscosity sense) can always be determined.

Under Assumptions 4.2, 4.3, 4.4 and 4.5, by Filippov's Theorem [22], the problem (20) admits an optimal solution, which implies the existence of an admissible $\mathbf{r}$ and $\mathbf{z}$ [14]. This yields the following relationship due to (18)

$$\bigvee_i J_{\mathrm{t}}^i(\mathbf{r}(0)) - \mathbf{z}^i(-t_f) = \bigvee_i J_{\mathrm{t}}^i(\mathbf{r}(0)) + \int_{-t_f}^{0} J_{\mathrm{r}}^i(\mathbf{r}(s), \mathbf{u}(s)) ds - z_0^i. \tag{24}$$

Let us now consider the case of minimizing z_0, such that $z_0 = J_{\mathrm{Bolza}}(\mathbf{r}, \mathbf{u}, t_f)$, which is naturally desirable in order to compute the objective function and subsequently the Pareto front in (22).

Proposition 4.3: Let $r_0 \in \mathbb{R}^7$ and $t_f \in [0,\infty)$. The value function $\vartheta(r_0, t_f, z_0)$ is such that

$$\forall z_0, \hat{z}_0 \in \mathbb{R}^p, z_0 \leq \hat{z}_0 \Rightarrow \vartheta(r_0, t_f, z_0) \geq \vartheta(r_0, t_f, \hat{z}_0).$$

Proof: Let $r_0 \in \mathbb{R}^7$ and $t_f \in [0,\infty)$ and $z_0, \hat{z}_0 \in \mathbb{R}^p$ with $z_0 \leq \hat{z}_0$. Since the infimum over $(\mathbf{r}, \mathbf{u}) \in \Pi_{r_0,t_f}$ is independent of z, due to Assumption 4.5 there exists a $(\mathbf{r}, \mathbf{u}) \in \Pi_{r_0,t_f}$, such that

$$\begin{aligned} &\vartheta(r_0, t_f, z_0) - \vartheta(r_0, t_f, \hat{z}_0) = \\ &\quad \bigvee_i J_{\mathrm{t}}^i(\mathbf{r}(0)) + \int_{-t_f}^{0} J_{\mathrm{r}}^i(\mathbf{r}(s), \mathbf{u}(s)) ds - z_0^i \\ &\quad \bigvee \nu(\mathbf{r}(0)) \bigvee \max_{s \in [-t_f, 0]} g(\mathbf{r}(s)) \\ &\quad - \bigvee_i J_{\mathrm{t}}^i(\mathbf{r}(0)) + \int_{-t_f}^{0} J_{\mathrm{r}}^i(\mathbf{r}(s), \mathbf{u}(s)) ds - \hat{z}_0^i \\ &\quad \bigvee \nu(\mathbf{r}(0)) \bigvee \max_{s \in [-t_f, 0]} g(\mathbf{r}(s)) \end{aligned}$$

Notice that if

$$\nu(\mathbf{r}(0)) \bigvee \max_{s \in [-t_f, 0]} g(\mathbf{r}(s)) \geq \bigvee_i J_{\mathrm{t}}^i(\mathbf{r}(0)) + \int_{-t_f}^{0} J_{\mathrm{r}}^i(\mathbf{r}(s), \mathbf{u}(s)) ds - z_0^i,$$

then since $z_0 \leq \hat{z}_0$, it also holds that

$$\nu(\mathbf{r}(0)) \bigvee \max_{s \in [-t_f, 0]} g(\mathbf{r}(s)) \geq \bigvee_i J_{\mathrm{t}}^i(\mathbf{r}(0)) + \int_{-t_f}^{0} J_{\mathrm{r}}^i(\mathbf{r}(s), \mathbf{u}(s)) ds - \hat{z}_0^i,$$

and hence $\vartheta(r_0, t_f, z_0) = \vartheta(r_0, t_f, \hat{z}_0)$. On the other hand, if

$$\nu(\mathbf{r}(0)) \bigvee \max_{s \in [-t_f, 0]} g(\mathbf{r}(s)) \leq \bigvee_i J_{\mathrm{t}}^i(\mathbf{r}(0)) + \int_{-t_f}^{0} J_{\mathrm{r}}^i(\mathbf{r}(s), \mathbf{u}(s)) ds - z_0^i,$$

Then it follows that

$$\begin{aligned} &\vartheta(r_0, t_f, z_0) - \vartheta(r_0, t_f, \hat{z}_0) = \\ &\quad \bigvee_i J_{\mathrm{t}}^i(\mathbf{r}(0)) + \int_{-t_f}^{0} J_{\mathrm{r}}^i(\mathbf{r}(s), \mathbf{u}(s)) ds - z_0^i \\ &\quad - \bigvee_i J_{\mathrm{t}}^i(\mathbf{r}(0)) + \int_{-t_f}^{0} J_{\mathrm{r}}^i(\mathbf{r}(s), \mathbf{u}(s)) ds - \hat{z}_0^i \\ &\qquad = \hat{z}_0^i - z_0^i \geq 0, \end{aligned}$$

which implies that

$$\vartheta(r_0, t_f, z_0) \geq \vartheta(r_0, t_f, \hat{z}_0),$$

thus concluding the proof. ■

As a consequence of the inverse relationship in Proposition 4.3, as we minimize z_0, we maximize the value function ϑ. If we assume that $\mathcal{K}$ is control invariant and $\mathcal{C}$ is open, then assuming a solution exists, i.e. $\Pi_{r_0,t_f}^{\mathcal{K},\mathcal{C}} \neq \emptyset$, the smallest upper bound for $J_{\mathrm{Bolza}}(\mathbf{r}, \mathbf{u}, t_f)$, leads to the largest ϑ that still admits an admissible solution, which is $\vartheta(r_0, t_f, z_0) = 0$. Consequently, we are able to turn the inequality constraint $\vartheta(r_0, t_f, z_0) \leq 0$ into an equality $\vartheta(r_0, t_f, z_0) = 0$. This leads to the following MOC problem for problems in Bolza form

$$\begin{aligned} \underset{(r_0,t_f) \in I \times [0,\infty)}{\text{minimize}} \quad & J_{\mathrm{Bolza}} \\ \text{subject to} \quad & \vartheta(r_0, t_f, J_{\mathrm{Bolza}}) = 0. \end{aligned} \tag{25}$$

Depending on the choice of solver, the equality constraint in (25) can lead to a significant increase in computational savings, as possible solutions can be neglected early on.

V. Numerical Approximation and Results

We will now discuss how the value functions can be obtained numerically, prior to discussing how the spacecraft trajectory design problem is solved. Following Proposition 4.1, a numerical solution to (23) can be found. To this end we employ the Level Set toolbox of [26]. For the computation of ω, we use a Lax-Friedrich Hamiltonian

$$\mathcal{H}(r, p^-, p^+) = H(r, \frac{p^- + p^+}{2}) - \sum_{k=1}^{7} \frac{\alpha_k}{2}(p^+ - p^-), \tag{26}$$

where p^+ and p^- are the right and left derivatives computed using an appropriate fifth-order weighted essentially non-oscillatory (WENO) scheme. The Lax-Friedrich Hamiltonian consists of an analytic expression of the Hamiltonian (derived previously), as well as a dissipation term, which is scaled by the dissipation coefficients α_k. The dissipation coefficients α_k needs to satisfy

$$\alpha_k \geq \left| \frac{\partial H}{\partial p_k} \right|. \tag{27}$$

Since we need α_k to serve as an upper bound, we consider the control input that maximizes the Hamiltonian:

$$\left|\frac{\partial H}{\partial p_k}\right| = \Big| -\frac{\partial C(r,q)}{\partial p_k} + \frac{\partial}{\partial p_k} \max\left(q_7 \cdot \frac{T_{\max}}{v_{\text{exhaust}}} + \frac{T_{\max}}{m_0 + \Delta m}\sqrt{q_4^2 + q_5^2 + q_6^2}, 0 \right) \Big| \tag{28}$$

$$\alpha_k = \begin{cases} |v_\rho| & k = 1 \\ |\frac{v_t}{\rho \sin\psi}| & k = 2 \\ |\frac{v_\perp}{\rho}| & k = 3 \\ |a_\rho - \max(0, \frac{T_{\max} q_3}{(m_0+\Delta m)\sqrt{q_3^2+q_4^2+q_5^2}})| & k = 4 \\ |a_t - \max(0, \frac{T_{\max} q_4}{(m_0+\Delta m)\sqrt{q_3^2+q_4^2+q_5^2}})| & k = 5 \\ |a_\perp - \max(0, \frac{T_{\max} q_5}{(m_0+\Delta m)\sqrt{q_3^2+q_4^2+q_5^2}})| & k = 6 \\ \frac{T_{\max}}{v_{\text{exhaust}}} & k = 7, \end{cases} \tag{29}$$

For a further discussion of the Lax-Friedrich Hamiltonian and WENO scheme, we refer to [27], while for a discussion of the convergence of ω and the derivation of a necessary Courant-Friedrichs-Lewy condition, we refer to [10], [26], [28].

A. Implementation

To illustrate the theoretical results of the previous sections, we consider a spacecraft on an initial circular orbit around asteroid Castalia 4769. The goal is to compute an efficient transfer trajectory that raises the orbit by 1 km. The gravity of Castalia 4769 was modeled by means of a spherical harmonic expansion as discussed in [29]–[31]. Furthermore, we consider only the planar case, omitting the states ψ and $v_\perp$.

To avoid ill-conditioning when solving the HJB equation, the state vector is normalized using the constants introduced in Table I. This results in the following dynamics:

$$\dot{r} = \begin{bmatrix} v_\rho \\ \frac{v_t}{\rho} \\ a_\rho + \frac{cT}{m_0+\Delta m}\cos\alpha \\ a_t + \frac{cT}{m_0+\Delta m}\sin\alpha \\ -\frac{cT}{v_{\text{exhaust}}} \end{bmatrix}, \tag{30}$$

where $c = T_{\max}\rho_0/(m_0 V_0^2)$ is a normalization constant. ρ_0, m_0 and v_0 denote the initial radius, mass and velocity of the initial orbit, respectively.

The optimal control policy and trajectory $(\mathbf{r}, \mathbf{u}) \in \Pi^{\mathcal{K},\mathcal{C}}_{r_0,t_f}$ can be constructed efficiently using the numerical approximation of ω. For a given $N \in \mathbb{N}$ we consider the timestep $h = \frac{1}{N}$ and a uniform grid of $[-t_f, 0]$ with spacing $s^k = \frac{k}{N}$. Let us define the state $\{r^k\}_{k=0}^{N}$ and control $\{u^k\}_{k=0}^{N-1}$ for the numerical approximation of the optimal trajectory and control policy. Setting r_0 as the initial orbit, we proceed by iteratively computing the control value

$$u^k(r^k) \in \arg\min_{u \in \mathcal{U}} \omega(r^k + hf(r^k, u), s^k) \bigvee g(r^k).$$

For a given $\omega(r^k, s^k)$ this is done by numerically taking the partial derivatives along each grid direction to estimate the costate vector q and then determining the optimal control value as the minimizer of the Hamiltonian H. After u^k is determined we compute r^{k+1} using an appropriate Adams-Bashforth-Moulton method [32] and increment k.

TABLE I
NORMALIZATION

Scale	Values
Distance	Initial radius ρ_0
Velocity	0.002 km/s
Time	ρ_0/v_0
Mass	10 kg
Force	Maximum thrust $T_{\max}$

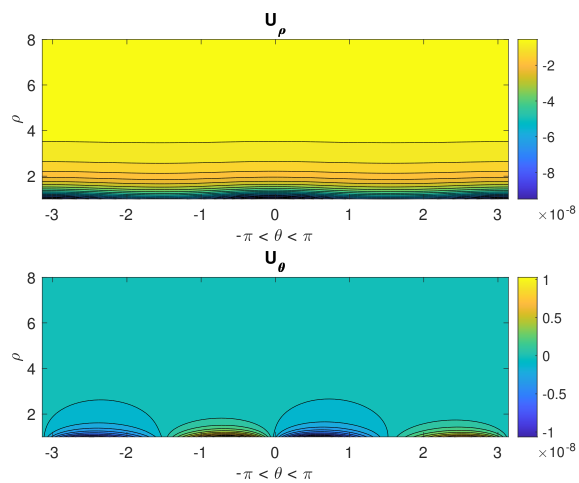

Fig. 1. Gravitational acceleration comparing U_ρ and U_θ around Castalia 4769.

As shown in Figure 1, when considering orbits further than 4 km away from the surface of the asteroid, the variation of the gravitational acceleration along θ becomes negligible. It is, therefore, possible to approximate the gravitational terms in spherical coordinates as

$$U_\rho(\rho, \theta) \approx U_\rho(\rho)$$
$$U_\theta(\rho, \theta) \approx 0.$$

Using this approximations makes a_ρ and a_t independent of θ. This allows us to omit a grid dimension while numerically solving the quasi-variational inequality in Theorem 4.2, greatly reducing the computational cost. Variable θ can easily be reconstructed during the trajectory construction, by simply integrating over the second dimension of $f(\mathbf{r}(t), \mathbf{u}(t))$.

B. Simulation results

The spacecraft is modeled with 750 kg of dry mass, 600 mN of maximum thrust and an exhaust velocity of 40 km/s. Using an initial orbit with radius 5.1 km and tangential velocity of -0.0024 km/s, we are able to compute the numerical approximation of ω using the grid described in Table II.

TABLE II
GRID CONFIGURATION

	ρ	v_ρ	v_t	Δm
Grid Points	32	24	24	16
Grid Spacing	0.0072	0.0693	0.0164	0.0143
Minimum	0.8047	-0.2772	-1.4457	-0.0571
Maximum	1.0289	1.3167	-1.0679	0.1571

The final computed trajectory, for an initial propellant mass of 0.06 kg and transfer time 2750 s is shown in Figure 4 with the propagation of the zero level set over time shown in Figure 2 and 3. The asteroid rendering for Figure 4 was computed as in [33].

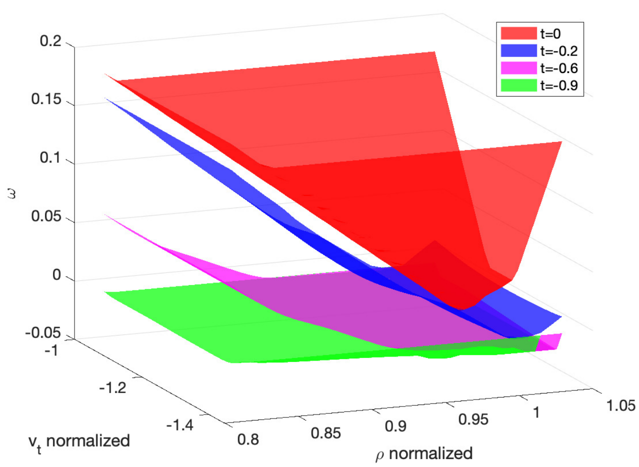

Fig. 2. The value function, ω, projected in the ρ-v_t plane for $v_\rho = 0$ and $\Delta m = 1$ kg.

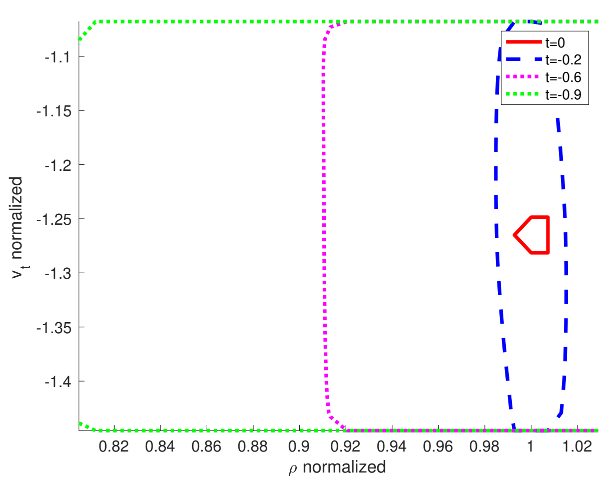

Fig. 3. The zero level set of the value function, ω, projected in the ρ-v_t plane for $v_\rho = 0$ and $\Delta m = 1$ kg.

The accuracy of the final orbit is within 73 meters and $6.19 \cdot 10^{-5}$ m/s of the target orbit. Calculating ω took 98 minutes using a 3 GHz 8-Core Intel Core i7-9700 processor running Matlab. The run time and accuracy can be significantly improved upon when using optimized code such as [34]–[36].

Once ω is computed, it is incorporate into (14), which is solved using Matlab's *paretosearch* function. Solving the MOC problem took 54 seconds and the resulting Pareto front is shown in Figure 5.

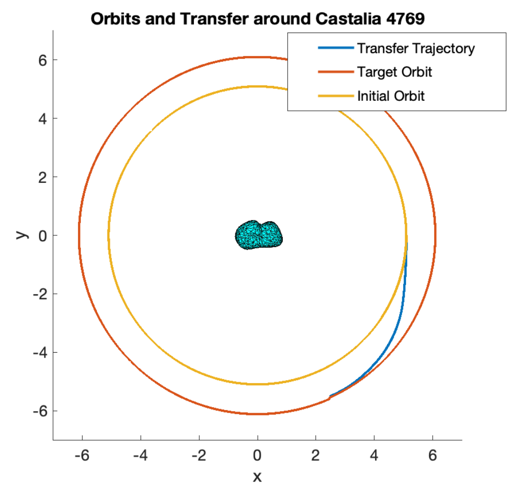

Fig. 4. Initial orbit and transfer trajectory to a circular orbit 1 km further away from the asteroid

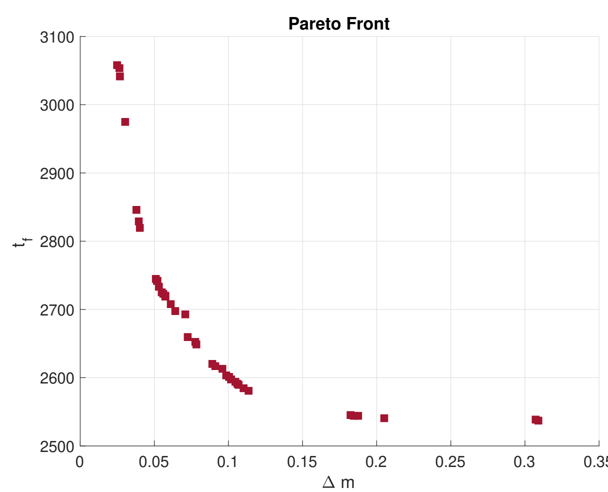

Fig. 5. Pareto front of the objective functions J_1 in kg and J_2 in seconds.

To illustrate the results of problems in Bolza form, we consider the case of optimizing the remaining propellant in oppose to the initial available propellant. Therefore, let us set the initial available propellant to 1 kg. We use a similar setup as in V, with the addition of the auxiliary state, z, defined as a terminal cost. We consider the uniform spaced grid over r and z, defined in Table III.

Since the objective is to maximize the remaining propellant, the optimization problem needs to minimize $-\Delta m$. Therefore, for a given final state $r_f \in \mathbb{R}^7$ and transfer time $t_f \in [0, +\infty)$, we define the cost functions as $J_1(r_f, t_f) := -\Delta m$ and

TABLE III
GRID CONFIGURATION FOR THE BOLZA PROBLEM

	ρ	v_ρ	v_t	Δm	z
Grid Points	32	24	24	16	18
Grid Spacing	0.0072	0.0693	0.0164	0.0143	0.0126
Minimum	0.8047	-0.2772	-1.4457	-0.0571	-0.1571
Maximum	1.0289	1.3167	-1.0679	0.1571	0.0571

$J_2(r_f, t_f) := t_f$, where Δm denotes the 7-th element of the state vector r_f (the mass in our case). The 2-dimensional objective function $J : \mathbb{R}^7 \times [0, +\infty) \to \mathbb{R}^2$ can then be written as

$$J(r_f, t_f) := [J_1(r_f, t_f), J_2(r_f, t_f)]^T . \tag{31}$$

The resulting Pareto front is shown in Figure 6. Calculating the reachable set took approximately 9 hours. Using the reachable set, calculating the Pareto front took approximately 135 seconds. As expected, the Pareto front looks similar to that of Figure 5, yet not identical due to numerical inaccuracy and change in the initial mass, resulting in modified dynamics.

Using an initial propellant mass of 1 kg, z of -0.9893 kg and transfer time of 2834 s, the transfer orbit is computed in the same way as before. As expected, the transfer trajectory is similar to the trajectory shown in Figure 4 and the accuracy of the transfer orbit is within 70 meters and $1.1 \cdot 10^{-3}$ m/s of the target orbit.

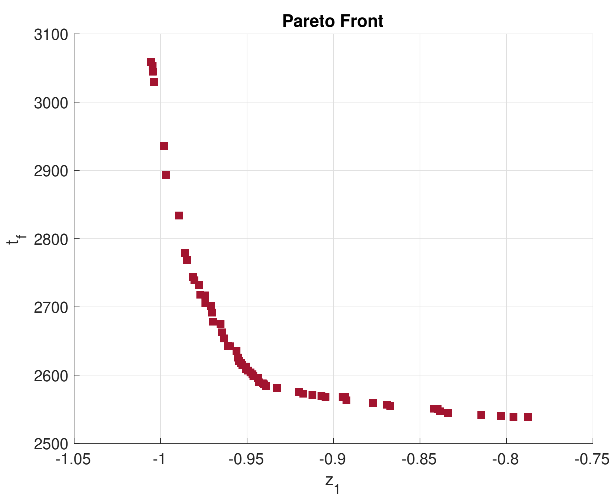

Fig. 6. Pareto front of the objective functions J_1 in kg and J_2 in seconds, for the Bolza problem.

VI. CONCLUSION

We have presented a novel method of using the value function of a quasi-variational inequality to compute the decision space of multi-objective optimization problems. The feasibility and effectiveness of the proposed approach was demonstrated by applying it to the problem of low-thrust trajectory design. The approach is applicable to arbitrary multi-objective optimization problems where the control variable is required to lie within a reachable set.

Future research concentrates utilizing approximations of the reachable set as in [37], as well as decomposed reachable sets [19] in order to generate initial guesses for MOC solvers. Since the extension to problems in Bolza form requires the addition of auxiliary states, utilizing research from high-dimensional reachability analysis, such as classification based approaches [38], deems promising.

APPENDIX

Proposition A.1: Under Assumption 4.2, any two trajectories $\mathbf{r}$ and $\hat{\mathbf{r}}$ reconstructed from f, with $\mathbf{r}(-t_f) = r_0$ and $\hat{\mathbf{r}}(-t_f) = \hat{r}_0$ respectively, are such that $||\mathbf{r}(\tau) - \hat{\mathbf{r}}(\tau)|| \leq ||r_0 - \hat{r}_0||e^{(t_f+\tau)L_f}$ for all $\tau \in [-t_f, 0]$.

Proof: Let $r_0, \hat{r}_0 \in \mathbb{R}^7$ be two initial states, and $t_f \in [0, \infty)$. For the same t_f, we choose two trajectory control pairs $(\mathbf{r}, \mathbf{u}) \in \Pi_{r_0,t_f}$ and $(\hat{\mathbf{r}}, \hat{\mathbf{u}}) \in \Pi_{\hat{r}_0,t_f}$. Then by Carathéodory's existence of solutions [21], the following relation holds:

$$\begin{aligned}
&||\mathbf{r}(-t) - \hat{\mathbf{r}}(-t)|| \leq \\
&\quad ||r_0 - \hat{r}_0|| + \int_{-t_f}^{-t} ||f(\mathbf{r}(s), \mathbf{u}(s)) - f(\hat{\mathbf{r}}(s), \hat{\mathbf{u}}(s))||ds \\
&\leq ||r_0 - \hat{r}_0|| + L_f \int_{-t_f}^{-t} ||\mathbf{r}(s) - \hat{\mathbf{r}}(s)||ds \leq ||r_0 - \hat{r}_0||e^{(t_f-t)L_f},
\end{aligned}$$

where the second inequality is due to Assumption 4.2, while the last inequality is due to the Bellman-Gronwall Lemma [21]. ■

A. Proof of Proposition 4.2

Proof: Fix $(r_0, z_0), (\hat{r}_0, \hat{z}_0) \in \mathbb{R}^7 \times \mathbb{R}^p$, $t_f \in [0, \infty)$ and let $\epsilon > 0$. We choose $(\hat{\mathbf{r}}, \hat{\mathbf{u}}, \hat{\mathbf{z}}) \in \mathcal{Z}_{\hat{r}_0,t_f,\hat{z}_0}$, such that

$$\begin{aligned}
\vartheta(\hat{r}_0, t_f, \hat{z}_0) \geq \bigvee_i J_{\mathrm{t}}^i(\hat{\mathbf{r}}(0)) - \hat{\mathbf{z}}^i(-t_f) \\
\bigvee \nu(\hat{\mathbf{r}}(0)) \bigvee \max_{s\in[-t_f,0]} g(\hat{\mathbf{r}}(s)) - \epsilon.
\end{aligned}$$

By definition of ϑ, for any $(\mathbf{r}, \mathbf{u}) \in \Pi_{r_0,t}$, this yields the following relation

$$\begin{aligned}
&\vartheta(r_0, t_f, z_0) - \vartheta(\hat{r}_0, t_f, \hat{z}_0) \\
&\quad \leq \bigvee_i J_{\mathrm{t}}^i(\mathbf{r}(0)) - \mathbf{z}^i(-t_f) \bigvee \nu(\mathbf{r}(0)) \bigvee \max_{s\in[-t_f,0]} g(\mathbf{r}(s)) \\
&- \bigvee_i J_{\mathrm{t}}^i(\hat{\mathbf{r}}(0)) - \hat{\mathbf{z}}^i(-t_f) \bigvee \nu(\hat{\mathbf{r}}(0)) \bigvee \max_{s\in[-t_f,0]} g(\hat{\mathbf{r}}(s)) + \epsilon.
\end{aligned}$$

Let $\kappa \in [-t_f, 0]$ be such that $g(\mathbf{r}(\kappa)) = \max_{s\in[-t_f,0]} g(\mathbf{r}(s))$. We then have

$$\begin{aligned}
&\vartheta(r_0, t_f, z_0) - \vartheta(\hat{r}_0, t_f, \hat{z}_0) \\
&\quad \leq \bigvee_i J_{\mathrm{t}}^i(\mathbf{r}(0)) - \mathbf{z}^i(-t_f) \bigvee \nu(\mathbf{r}(0)) \bigvee g(\mathbf{r}(\kappa)) \\
&\quad - \bigvee_i J_{\mathrm{t}}^i(\hat{\mathbf{r}}(0)) - \hat{\mathbf{z}}^i(-t_f) \bigvee \nu(\hat{\mathbf{r}}(0)) \bigvee g(\hat{\mathbf{r}}(\kappa)) + \epsilon.
\end{aligned}$$

Using Proposition A.1, we distinguish the following cases.

Case A: $g(\mathbf{r}(\kappa)) \geq \bigvee_i J_{\mathrm{t}}^i(\mathbf{r}(0)) - \mathbf{z}^i(-t_f) \bigvee \nu(\mathbf{r}(0))$

$$\begin{aligned}
&\vartheta(r_0, t_f, z_0) - \vartheta(\hat{r}_0, t_f, \hat{z}_0) \\
&\leq g(\mathbf{r}(\kappa)) - \bigvee_i J_{\mathrm{t}}^i(\hat{\mathbf{r}}(0)) - \hat{\mathbf{z}}^i(-t_f) \bigvee \nu(\hat{\mathbf{r}}(0)) \bigvee g(\hat{\mathbf{r}}(\kappa)) + \epsilon \\
&\quad \leq g(\mathbf{r}(\kappa)) - g(\hat{\mathbf{r}}(\kappa)) + \epsilon \leq L_g e^{(t_f+\kappa)L_f}||r_0 - \hat{r}_0|| + \epsilon,
\end{aligned}$$

where the last inequality is due to the face that g is Lipschitz continuous.

Case B: $\nu(\mathbf{r}(0)) \geq \bigvee_i J_{\mathrm{t}}^i(\mathbf{r}(0)) - \mathbf{z}^i(-t_f) \bigvee g(\mathbf{r}(\kappa))$

$$\begin{aligned}
&\vartheta(r_0, t_f, z_0) - \vartheta(\hat{r}_0, t_f, \hat{z}_0) \\
&\leq \nu(\mathbf{r}(0)) - \bigvee_i J_{\mathrm{t}}^i(\hat{\mathbf{r}}(0)) - \hat{\mathbf{z}}^i(-t_f) \bigvee \nu(\hat{\mathbf{r}}(0)) \bigvee g(\hat{\mathbf{r}}(\kappa)) + \epsilon \\
&\leq \nu(\mathbf{r}(0)) - \nu(\hat{\mathbf{r}}(0)) + \epsilon \leq L_\nu e^{t_f L_f} ||r_0 - \hat{r}_0|| + \epsilon
\end{aligned}$$

Case C: $\bigvee_i J_{\mathrm{t}}^i(\mathbf{r}(0)) - \mathbf{z}^i(-t_f) \geq g(\mathbf{r}(\kappa)) \bigvee \nu(\mathbf{r}(0))$
Recall (24), then under Assumption 4.2, any two trajectories $\mathbf{z}$ and $\hat{\mathbf{z}}$ reconstructed from J_{r} with z_0 and $\hat{z}_0$, respectively, are bounded within a given time interval $[-t, 0]$. To see this,

$$\begin{aligned}
&||\mathbf{z}(-t) - \hat{\mathbf{z}}(-t)|| \\
&\leq ||z_0 - \hat{z}_0|| + \int_{-t}^{0} ||J_{\mathrm{r}}(\mathbf{r}(s), \mathbf{u}(s)) - J_{\mathrm{r}}(\hat{\mathbf{r}}(s), \hat{\mathbf{u}}(s))|| ds \\
&\leq ||z_0 - \hat{z}_0|| + L_{\mathrm{r}} \int_{-t}^{0} ||\mathbf{r}(s) - \hat{\mathbf{r}}(s)|| ds \\
&\leq ||z_0 - \hat{z}_0|| + L_{\mathrm{r}} \int_{-t}^{0} ||r_0 - \hat{r}_0|| e^{(t_f + s) L_f} ds \\
&\leq ||z_0 - \hat{z}_0|| + ||r_0 - \hat{r}_0|| L_{\mathrm{r}} e^{t_f L_f} \frac{1 - e^{-t L_f}}{L_f},
\end{aligned}$$

where the third inequity is due to Proposition A.1, and the last one follows by performing the integration.

Next, let $j \in [1, \ldots, p]$ be such that

$$J_{\mathrm{t}}^j(\mathbf{r}(0)) - \mathbf{z}^j(-t_f) = \bigvee_i J_{\mathrm{t}}^i(\mathbf{r}(0)) - \mathbf{z}^i(-t_f).$$

Then it follows, that

$$\begin{aligned}
&\vartheta(r_0, t_f, z_0) - \vartheta(\hat{r}_0, t_f, \hat{z}_0) \leq \\
&\qquad \leq \bigvee_i J_{\mathrm{t}}^i(\mathbf{r}(0)) - \mathbf{z}^i(-t_f) - \\
&\quad \bigvee_i J_{\mathrm{t}}^i(\hat{\mathbf{r}}(0)) - \hat{\mathbf{z}}^i(-t_f) \bigvee \nu(\hat{\mathbf{r}}(0)) \bigvee g(\hat{\mathbf{r}}(\kappa)) + \epsilon \\
&\leq \bigvee_i J_{\mathrm{t}}^i(\mathbf{r}(0)) - \mathbf{z}^i(-t_f) - \bigvee_i J_{\mathrm{t}}^i(\hat{\mathbf{r}}(0)) - \hat{\mathbf{z}}^i(-t_f) + \epsilon \\
&\leq \Big[J_{\mathrm{t}}^j(\mathbf{r}(0)) - \mathbf{z}^j(-t_f)\Big] - \Big[J_{\mathrm{t}}^j(\hat{\mathbf{r}}(0)) - \hat{\mathbf{z}}^j(-t_f)\Big] + \epsilon \\
&\leq \Big[J_{\mathrm{t}}^j(\mathbf{r}(0)) - J_{\mathrm{t}}^j(\hat{\mathbf{r}}(0))\Big] - \big[\mathbf{z}^j(-t_f) - \hat{\mathbf{z}}^j(-t_f)\big] + \epsilon
\end{aligned}$$

By Proposition A.1 and under Assumption 4.3

$$\Big[J_{\mathrm{t}}^j(\mathbf{r}(0)) - J_{\mathrm{t}}^j(\hat{\mathbf{r}}(0))\Big] \leq L_{\mathrm{t}} ||r_0 - \hat{r}_0|| e^{t_f L_f}.$$

Finally, this yields the relationship

$$\begin{aligned}
&\Big[J_{\mathrm{t}}^j(\mathbf{r}(0)) - J_{\mathrm{t}}^j(\hat{\mathbf{r}}(0))\Big] - \big[\mathbf{z}^j(-t_f) - \hat{\mathbf{z}}^j(-t_f)\big] + \epsilon \\
&\leq ||z_0 - \hat{z}_0|| + ||r_0 - \hat{r}_0|| \Big[L_{\mathrm{t}} e^{t_f L_f} + L_{\mathrm{r}} \frac{e^{t_f L_f} - 1}{L_f}\Big] + \epsilon.
\end{aligned}$$

Thus in every case, on an interval $[0, t_f]$ there exists a set of constants C_r and C_z, such that

$$\vartheta(r_0, t_f, z_0) - \vartheta(\hat{r}_0, t_f, \hat{z}_0) \leq C_r ||r_0 - \hat{r}_0|| + C_z ||z_0 - \hat{z}_0|| + \epsilon$$

The same argument conducted with (r_0, t_f, z) and $(\hat{t}_f, \hat{r}_0, \hat{z})$ reversed establishes that

$$\vartheta(\hat{r}_0, t_f, \hat{z}_0) - \vartheta(r_0, t_f, z_0) \leq C_r ||r_0 - \hat{r}_0|| + C_z ||z_0 - \hat{z}_0|| + \epsilon.$$

Since ϵ is arbitrary, we conclude that

$$||\vartheta(\hat{r}_0, t_f, \hat{z}_0) - \vartheta(r_0, t_f, z_0)|| \leq C_r ||r_0 - \hat{r}_0|| + C_z ||z_0 - \hat{z}_0||,$$

thus concluding the proof. ■

The proof for ω is similar to that of ϑ and we will therefore omit it in the interest of space.

REFERENCES

[1] P. G. Antreasian, F. T. Nicholson, P. H. Kallemeyn, S. Bhaskaran, R. J. Haw, and P. Halamek, "Galileo orbit determination for the Ida encounter," *Advances in the Astronautical Sciences*, vol. 87, no. 2, pp. 1027–1048, 1994.

[2] D. W. Parcher, "Low-thrust orbit transfer design for Dawn operations at Vesta," *Advances in the Astronautical Sciences*, vol. 140, no. 818, pp. 1213–1232, 2011.

[3] M. J. Abrahamson, A. Ardito, D. Han, R. Haw, B. Kennedy, N. Mastrodemos, S. Nandi, R. Park, B. Rush, and A. Vaughan, "Dawn orbit determination team: Trajectory modeling and reconstruction processes at Vesta," *Advances in the Astronautical Sciences*, vol. 148, no. February, pp. 2271–2290, 2013.

[4] S. Ober-Blöbaum, M. Ringkamp, and G. zum Felde, "Solving multiobjective optimal control problems in space mission design using discrete mechanics and reference point techniques," in *2012 IEEE 51st IEEE Conference on Decision and Control (CDC)*, 2012, pp. 5711–5716.

[5] J. P. Aubin, J. Lygeros, M. Quincampoix, S. Sastry, and N. Seube, "Impulse differential inclusions: A viability approach to hybrid systems," *IEEE Transactions on Automatic Control*, vol. 47, no. 1, pp. 2–20, 2002.

[6] J. Lygeros, C. Tomlin, and S. Sastry, "Controllers for reachability specifications for hybrid systems," *Automatica*, vol. 35, no. 3, pp. 349–370, 1999.

[7] I. M. Mitchell, A. M. Bayen, and C. J. Tomlin, "A time-dependent Hamilton-Jacobi formulation of reachable sets for continuous dynamic games," *IEEE Transactions on Automatic Control*, vol. 50, no. 7, pp. 947–957, 2005.

[8] K. Margellos and J. Lygeros, "Hamilton-jacobi formulation for reach-avoid differential games," *IEEE Transactions on Automatic Control*, vol. 56, no. 8, pp. 1849–1861, aug 2011.

[9] ——, "Toward 4-D trajectory management in air traffic control: A study based on monte carlo simulation and reachability analysis," *IEEE Transactions on Control Systems Technology*, vol. 21, no. 5, pp. 1820–1833, 2013.

[10] O. Bokanowski, N. Forcadel, and H. Zidani, "Reachability and minimal times for state constrained nonlinear problems without any controllability assumption," *SIAM Journal on Control and Optimization*, vol. 48, no. 7, pp. pp. 4292–4316, 2010.

[11] O. Bokanowski, E. Bourgeois, A. Désilles, and H. Zidani, "Payload optimization for multi-stage launchers using HJB approach and application to a SSO mission," *IFAC-PapersOnLine*, vol. 50, no. 1, pp. 2904–2910, 2017.

[12] O. Bokanowski, E. Bourgeois, A. Désilles, and H. Zidani, "Global optimization approach for the climbing problem of multi-stage launchers ," Feb. 2015, working paper or preprint. [Online]. Available: https://hal-ensta-paris.archives-ouvertes.fr//hal-01113819

[13] J. F. Fisac, M. Chen, C. J. Tomlin, and S. S. Sastry, "Reach-avoid problems with time-varying dynamics, targets and constraints," in *Proceedings of the 18th International Conference on Hybrid Systems: Computation and Control*, ser. HSCC '15. New York, NY, USA: Association for Computing Machinery, 2015, p. 11–20.

[14] A. Désilles and H. Zidani, "Pareto front characterization for multiobjective optimal control problems using Hamilton-Jacobi approach," *SIAM Journal on Control and Optimization*, vol. 57, no. 6, pp. 3884–3910, 2019.

[15] N. Vertovec, S. Ober-Blöbaum, and K. Margellos, "Multi-objective minimum time optimal control for low-thrust trajectory design," in *2021 European Control Conference (ECC)*, 2021.

[16] D. C. Redding and J. V. Breakwell, "Optimal low-thrust transfers to synchronous orbit," *Journal of Guidance, Control, and Dynamics*, vol. 7, no. 2, pp. 148–155, 1984.

[17] Y. Jiang and H. Baoyin, "Orbital Mechanics near a Rotating Asteroid," *Journal of Astrophysics and Astronomy*, 2014.
[18] D. T. Greenwood, *Principles of dynamics*, 2nd ed. Englewood Cliffs, N.J: Prentice-Hall, 1988.
[19] M. Chen, S. L. Herbert, M. S. Vashishtha, S. Bansal, and C. J. Tomlin, "Decomposition of Reachable Sets and Tubes for a Class of Nonlinear Systems," *IEEE Transactions on Automatic Control*, vol. 63, no. 11, 2018.
[20] K. Miettinen, *Nonlinear Multiobjective Optimization*, ser. International Series in Operations Research & Management Science. Boston, MA: Springer US, 1998, vol. 12.
[21] S. Sastry, *Nonlinear systems : analysis, stability, and control*, ser. Interdisciplinary applied mathematics ; v. 10. New York ; London: Springer, 1999.
[22] D. Liberzon, *Calculus of variations and optimal control theory: A concise introduction*. Princeton University Press, 2011.
[23] Bardi, Martino and Capuzzo-Dolcetta, Italo, *Optimal Control and Viscosity Solutions of Hamilton-Jacobi-Bellman Equations*. Birkhäuser Basel, 1997.
[24] A. Altarovici, O. Bokanowski, and H. Zidani, "A general Hamilton-Jacobi framework for non-linear state-constrained control problems," *ESAIM - Control, Optimisation and Calculus of Variations*, vol. 19, no. 2, pp. 337–357, 2013.
[25] W. Dahmen and A. Reusken, *Numerik für Ingenieure und Naturwissenschaftler*. Springer, 2008.
[26] I. M. Mitchell, "The flexible, extensible and efficient toolbox of level set methods," *Journal of Scientific Computing*, vol. 35, no. 2-3, pp. 300–329, 2008.
[27] S. Osher and R. Fedkiw, *Level Set Methods and Dynamic Implicit Surfaces*, ser. Applied Mathematical Sciences. Springer New York, 2003.
[28] C. Hermosilla, P. R. Wolenski, and H. Zidani, "The Mayer and Minimum Time Problems with Stratified State Constraints," *Set-Valued and Variational Analysis*, vol. 26, no. 3, pp. 643–662, 2018.
[29] R. S. Hudson and S. J. Ostro, "Shape of asteroid 4769 Castalia (1989 PB) from inversion of radar images," *Science*, 1994.
[30] D. J. Scheeres, J. K. Miller, and D. K. Yeomans, "The Orbital Dynamics Environment of 433 Eros: A Case Study for Future Asteroid Missions," *BBA - Bioenergetics*, 1987.
[31] D. J. Scheeres, S. J. Ostro, R. S. Hudson, and R. A. Werner, "Orbits close to asteroid 4769 Castalia," *Icarus*, vol. 121, no. 1, pp. 67–87, 1996.
[32] L. F. Shampine and M. W. Reichelt, "The MATLAB ODE Suite," *SIAM Journal on Scientific Computing*, vol. 18, no. 1, pp. 1–22, jan 1997.
[33] S. Kulumani and T. Lee, "Low-thrust trajectory design using reachability sets near asteroid 4769 Castalia," *AIAA/AAS Astrodynamics Specialist Conference, 2016*, pp. 1–12, 2016.
[34] O. Bokanowski, A. Désilles, H. Zidani, and J. Zhao, "ROC-HJ solver." [Online]. Available: https://uma.ensta-paris.fr/soft/ROC-HJ/
[35] M. Chen, S. Herbert, S. Bansal, and C. Tomlin, "Optimal control helper toolbox." [Online]. Available: https://github.com/HJReachability/helperOC
[36] M. Chen, J. Fisac, and C. Tomlin, "Berkeley efficient api in c++ for level set methods." [Online]. Available: https://github.com/HJReachability/beacls
[37] S. Bansal and C. J. Tomlin, "Deepreach: A deep learning approach to high-dimensional reachability," *CoRR*, vol. abs/2011.02082, 2020.
[38] V. Rubies-Royo, D. Fridovich-Keil, S. Herbert, and C. J. Tomlin, "A classification-based approach for approximate reachability," *Proceedings - IEEE International Conference on Robotics and Automation*, vol. 2019-May, pp. 7697–7704, 2019.